

Modeling the hallmarks of avascular tumors

Erik Blom^[0009-0005-8141-6802] and
Stefan Engblom^[0000-0002-3614-1732] and
Gesina Menz^[0000-0002-3589-9824]

Abstract We present a stochastic computational model of avascular tumors, emphasizing the detailed implementation of the first four so-called hallmarks of cancer: self-sufficiency in growth factors, resistance to growth inhibitors, avoidance of apoptosis, and unlimited growth potential. Our goal is to provide a foundational understanding of the first steps of cancer malignancy while addressing modeling uncertainties, thus bringing us closer to a first-principles grasp of this process. Preliminary numerical simulations illustrate the comprehensiveness of our perspective.

1 Introduction

Cancer, a complex and multifaceted disease, has been characterized by specific acquired capabilities underlying its progression [8]. These *hallmarks of cancer*, introduced by Hanahan and Weinberg, aim to aid the understanding of the disease complexity by providing a limited number of fundamental characteristics which establish a *conceptual scaffold* for cancer research [7]. The original six hallmarks describe different ways in which cells evade normal regulatory processes and attain features such as vascularization to ensure the continued survival of a malignant tumor. They can occur in a variable order and due to differing underlying cellular processes depending on the specific cancer type.

By distilling cancer characteristics to a limited few overarching processes, Hanahan and Weinberg's hope was to enable researchers and clinicians to specifically target aspects of cancer developments through therapeutic measures. This goal of clinical application, however, has only proven moderately successful due to the high variability in pathways through which each individual hallmark can be achieved [7].

Erik Blom, Stefan Engblom, and Gesina Menz
Division of Scientific Computing, Department of Information Technology, Uppsala university, e-mail: erik.blom@it.uu.se, e-mail: stefane@it.uu.se, e-mail: gesina.menz@it.uu.se

Indeed, criticism against the hallmark concept has been voiced in this context, stating that the low therapeutic success is due to focusing too much on cell-based events and, thus, oversimplifying the complexity of cancer as a tissue-level disease [10]. Nevertheless, the hallmarks are a widely accepted framework within the field of oncological research and have given researchers a reasonably defined yet simple framework for further research since their introduction.

One such avenue for further research is the use of modeling. There is promising potential in furthering our understanding of a diverse range of biological phenomena from carefully constructed computational models, e.g., tumor growth laws [1] and immune response [5]. Such models supplement biological experiments as they provide means to test hypotheses while controlling for biological variability, can propose new experiments and allow for new insights such as deciphering causal relationships between different pathways [3].

Motivated by the utility and precision of mathematical models, we aim to sharpen our understanding of cancer by interpreting its hallmarks into an *in silico* setting. Not only does this computational version of the hallmarks serve as a way to sharpen their formulation by making them quantitatively testable [3], but we also assess the overall usefulness and expressibility of our computational framework [6].

Our work in this paper revolves around implementing the first four hallmarks of cancer. In §2 we describe our modeling framework along with the specifics required to delineate each hallmark. In §3 we report some results from the resulting numerical simulations and a concluding discussion is found in §4.

2 Methods

We interpret the first four hallmarks of cancer into an existing stochastic and cell-based framework for avascular tumor growth [6], allowing for the study of the transition from healthy homeostasis to the early stages of cancer. The computational framework is summarized in §2.1 and the hallmark-specific mechanisms are developed in §2.2.

2.1 Stochastic modeling framework

Our model is an extension of the avascular tumor model in [2], which is based on the Darcy’s Law Cell Mechanics (DLCM) framework, in which cells are explicitly represented and their states updated in a continuous-time Markov chain [6].

Let Ω denote the tissue domain populated with cells and let Ω_{comp} denote the entire computational domain including the space with no cells. In Ω , cell migration for cell density u is governed by Darcy’s law [11] for fluid flow through porous media

$$\mathbf{v} = -D\nabla p, \tag{1}$$

where p is the pressure and the constant D is the the ratio of the medium permeability to its dynamic viscosity. The pressure is governed by a stationary heat equation with sources corresponding to crowding:

$$\left. \begin{aligned} -\Delta p &= s(u), \\ p &= p^{(\text{ext})} - \sigma C, \end{aligned} \right\} \quad \text{on } \partial\Omega \quad (2)$$

where $s(u)$ is a source function to be defined, $p^{(\text{ext})}$ is the pressure outside the cell population, C the population boundary curvature, and σ the surface tension coefficient. Cells are represented as discrete units in a computational mesh, and pressure sources arise only in voxels that exceed a *carrying capacity*, here defined as one cell per voxel. While the original framework considers cell proliferation and death as determined by an underlying nutrient field, to limit the model complexity we here consider that the cells always have sufficient nutrients for proliferation.

The domain is discretized into voxels v_i for $i = 1, 2, \dots, N_{\text{vox}}$ with total number of cells N_{cells} . The number of cells in a voxel is restricted to $u_i \in \{0, 1, 2\}$, and we define $s(u_i) = 1$ in (2) in v_i if $u_i > 1$ and zero otherwise. A cell can take on alternative phenotypes, e.g., necrotic or senescent, and are then equipped with behavior distinct from regular cells, here distinguished by a superscript as in $u_i^{(l)}$. Let $P(\omega)$ denote the rate of an event ω , and let cell migration from voxel v_i to v_j be denoted $i \rightarrow j$. The following movement events based on (1) are included

$$\left. \begin{aligned} P(i \rightarrow j; u_i \geq 1, u_j = 0) &= D_1 q_{ij} \\ P(i \rightarrow j; u_i > 1, u_j = 1) &= D_2 q_{ij} \end{aligned} \right\} \quad (3)$$

where D_1 and D_2 are the Darcy coefficients for respective movement type and q_{ij} is the pressure gradient integrated over the boundary shared between the voxels v_i and v_j . All the rates in this framework are interpreted as competing Poissonian events and simulated by suitable algorithms.

2.2 The hallmarks of cancer *in silico*

Although the framework in §2.1 supports basic tumor models, it does not make the hallmarks of cancer explicit. To study these we must therefore detail their mechanisms. A constraint that we impose is that they should endow benign cell populations with the capacity to maintain homeostasis.

We next describe how each of these four hallmarks are interpreted into the model.

2.2.1 Self-sufficiency in growth factors

Healthy cells spend most of their time in a non-replicative state and rely on growth signals to induce replication. Tumors, however, are much less dependent on external signaling and are able to proliferate in the absence of such environmental cues [8].

While the signaling network for initiating cell growth and proliferation is complex [9], we shall consider only short range growth signals induced within regions of low cell density such that a population of healthy cells can return to homeostasis after a cell loss. The growth signals are modeled as a quantity g governed by

$$\left. \begin{aligned} -\Delta g &= s_g(v_i) - \gamma g \\ g &= 0, \quad \text{on } \partial\Omega_{\text{comp}} \end{aligned} \right\} \quad (4)$$

with $s_g(v_i) = 1$ if v_i is empty and zero otherwise. We include the condition $g \geq g_{\text{prol},i}$ required for proliferation of cell i , where g_{prol} and γ together control the effective range of the growth signal g . To estimate suitable values of g_{prol} and γ we solve (4) in the radially symmetric case when only a single center voxel is empty and for cell diameter h . For large enough values of γ and for $r \geq 0.5h$,

$$g(r) = \frac{0.5h}{\sqrt{\gamma}} I_0(\sqrt{\gamma}h) K_0(\sqrt{\gamma}r), \quad (5)$$

in terms of modified Bessel functions of the first and second kind. To arrive at an estimate, we impose that $g_{\text{prol}} = g(h) = 4g(2h)$, such that the first layer of cells surrounding an empty voxel may proliferate and that the second layer of cells requires roughly three more empty voxels at equal distance to proliferate. For example, using $h = 0.04$, this condition is satisfied when $\gamma \approx 700$ and $g_{\text{prol}} \approx 8 \times 10^{-5}$.

2.2.2 Bypassing suppressive growth signals

As described in §2.2.1, cells in healthy tissues are assumed to spend the major parts of their lives in quiescence. This is induced by the immediate surroundings of individual cells releasing antigrowth signals to sustain tissue homeostasis. Tumor cells are able to evade this external feedback by disrupting or completely blocking pathways monitoring the received signals [8].

We introduce a local sensing mechanism by imposing the proliferation condition $e < e_{\text{prol},i}$ for cell i , where e is defined as the weighted voxel edge ratio

$$e = \frac{\sum_{j \in N_i} u_j E_{ij}}{\sum_{j \in N_i} E_{ij}}, \quad (6)$$

where E_{ij} is the edge length shared between v_i and v_j , and N_i is the set of all neighboring voxels to v_i . Thus, cell proliferation is suppressed so long as a certain fraction of the cell's boundary is adjacent to other cells.

2.2.3 Avoiding apoptosis

Apart from quiescence, healthy tissues also require apoptosis to maintain tissue homeostasis. If cells experience high levels of stress such as DNA damage or over-

crowding, the apoptotic pathway can be triggered to protect the tissue by reducing overall stress levels. It is therefore advantageous for cancers to be able to evade apoptosis to ensure continued proliferation even when cellular stress is high [9].

We assume that all living cells are equally likely to sustain spontaneous cell damage enough to initiate apoptosis: this is covered by a small background death rate $\epsilon\mu_{\text{apopt},i}$ for each cell i . We judge that signal imbalance occurs for cells i with $g < g_{\text{prol},i}$ or $e \geq e_{\text{prol},i}$ in voxels where $u_i > 1$. In other words, a recently proliferated cell with incoming signals which are in conflict with a proliferation event would trigger this signal imbalance. Finally, we measure DNA damage by the deviation of the first two cell-specific hallmark parameters $\theta_i = [g_{\text{prol},i}, e_{\text{prol},i}]$ from their corresponding healthy values $\theta_0 = [g_{\text{prol},0}, e_{\text{prol},0}]$, and we assume that both signal imbalance and DNA damage induce apoptosis at a rate proportional to $\mu_{\text{apopt},i}$ as specified in §2.2.4 below.

2.2.4 Unlimited growth potential

While the three previous hallmarks help tumor grow by decoupling cell proliferation from external signals, an additional requirement for the development of macroscopic tumors is the loss of replicative limitations. Healthy cells generally have the capacity to proliferate only a finite number of times. Cancer cells, however, are often able to replicate infinitely often [8, 9].

To achieve this in our model, we equip each cell i with a number η_i such that cells with $\eta_i = 0$ can no longer proliferate. After proliferation, each daughter cell inherits the value of η_i reduced by one, and we include a possibility of mutating this value and the other hallmark phenotypes as described in §3 below.

Including proliferation and degradation events, all event rates thus read as

$$\left. \begin{aligned} P(u_i \rightarrow u_i + 1; \text{cond}_{\text{prol}}) &= \mu_{\text{prol}}u_i \\ P(u_i \rightarrow u_i^{(\text{necr})}) &= \mu_{\text{apopt},i}u_i (\epsilon + d(\theta_i, \theta_0)) \\ P(u_i \rightarrow u_i^{(\text{necr})}; \text{cond}_{\text{apopt}}) &= \mu_{\text{apopt},i}u_i, \\ P(u_i^{(\text{necr})} \rightarrow u_i^{(\text{necr})} - 1) &= \mu_{\text{deg}}u_i^{(\text{necr})}, \end{aligned} \right\} \quad (7)$$

$$\text{where } \text{cond}_{\text{prol}} \text{ is } u_i < 2, g \geq g_{\text{prol},i}, e < e_{\text{prol},i}, \eta_i > 0, \quad (8)$$

$$\text{and where } \text{cond}_{\text{apopt}} \text{ is } u_i > 1, g < g_{\text{prol},i} \text{ or } e \geq e_{\text{prol},i}, \quad (9)$$

and $d(\cdot, \cdot)$ is the l_2 -distance in the parameter space. To simplify the implementation we impose $u_i^{(\text{necr})} \leq 1$ by letting death events in voxels with $u_i > 1$ simply remove the cell instead of it becoming necrotic.

In this way the first four *in silico* hallmarks are achieved in the limit when $g_{\text{prol}} \rightarrow 0$, $e_{\text{prol}} \rightarrow 1$, $\mu_{\text{apopt}} \rightarrow 0$, and when η is sufficiently large for the considered tumor timescale. The model parameters are summarized in Tab. 1.

Parameter	Description
$D_1 = 1$	Ratio medium permeability to dynamic viscosity [$f^{-1}l^3t^{-1}$]
$D_2 = 25$	As D_1 , but movement from doubly to singly occupied voxel
$\mu_{\text{prol}} = 1$	Rate of cell proliferation [t^{-1}]
$\mu_{\text{death}} = 1$	Rate of cell death [t^{-1}]
$\mu_{\text{deg}} = 0.1$	Rate of dead cell degradation [t^{-1}]
$\sigma = 10^{-4}$	Surface tension coefficient [f]
$\gamma = 500$	Ratio of growth signal decay to diffusion rate [l^{-2}]
$\epsilon = 5 \times 10^{-3}$	Background apoptosis rate factor [-]
$g_{\text{prol},0} = 10^{-4}$	Healthy growth signalling threshold [l^{-2}]
$e_{\text{prol},0} = 1$	Healthy anti-growth signalling threshold [-]
$\mu_{\text{apopt},0} = 0.25$	Healthy apoptosis rate [t^{-1}]
$\eta_0 = 20$	Healthy cell proliferation number [-]

Table 1 Cell population model parameters. The units (t , l , f) correspond to units of time, length, and force, respectively.

3 Numerical results

We focus here on a numerical illustration that provides insight into the model's capacity to capture the transition from normal tissue to malignancy, thus offering a fairly detailed depiction of the early stages of cancer development.

We monitor the overall *tumor reproduction number* R_{pop} defined as the population mean of the cells' expected number R_i of proliferation events before death. To find R_i for cell i , we consider the equivalent branching process of a sequence of Bernoulli trials with probability q_i for a proliferation event and $p_i \equiv 1 - q_i$ for a death event that ends the process. We identify the proliferation probability with the total instantaneous proliferation- and death rates, b_i and d_i , respectively, according to $q_i = b_i / (b_i + d_i)$. However, we let $q_i = 0$ for the final step of the sequence after η_i proliferation events have occurred to account for the known limit of each cell's growth potential. The expected number of proliferation events of this branching process is

$$R_i = \sum_{j=0}^{\eta_i-1} j q_i^j (1 - q_i) + \eta_i q_i^{\eta_i} = q_i \frac{1 - q_i^{\eta_i}}{1 - q_i}. \quad (10)$$

Taking the population mean of this we arrive at the reproduction number

$$R_{\text{pop}} = N_{\text{cells}}^{-1} \sum_i \frac{b_i}{d_i} (1 - q_i^{\eta_i}). \quad (11)$$

We use the parameter values in Tab. 1 where we set the initial hallmark parameters for all cells to respective *healthy* parameter values. We include the probability $\alpha_4 = 10^{-3}$ that η_i increases by 1000 at cell division, and let the other three hallmark phenotypes mutate at cell division to study the selection pressure on the hallmark capabilities. The mutation process for the first three hallmark phenotypes is a drift-free geometric Brownian motion in phenotype space with diffusion coefficient equal to $\alpha_i = 0.2$ for

$i = 1, 2, 3$, rejecting values outside the domain of validity for each phenotype. We induce a higher cellular turnover by imposing necrosis at rate μ_{death} for cells in the central region $r \leq 0.2$ of the population to increase the effective mutation rates. The initial state is $u_i = 1$ everywhere in a circular domain of unit radius, discretized by a Cartesian mesh with voxel size $h = 0.04$.

Fig. 1 Population reproduction number (“fitness”) with the shaded grey area indicating ± 1 standard deviation, together with the status of each hallmark during one simulation. Mutation rates for the second and third hallmark capabilities are activated after $t = 100$ and 200 , respectively. The hallmarks are represented by the population mean of the corresponding hallmark parameter mapped to $[0, 1]$.

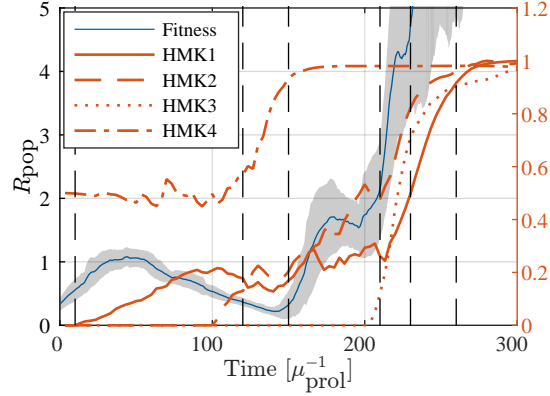


Fig. 1 summarizes the results of one simulation, including the population means of respective hallmark parameter (denoted by bars) mapped to $[0, 1]$ via $1 - \bar{g}_{\text{prol}}/g_{\text{prol},0}$, $\bar{e}_{\text{prol}}/e_{\text{prol},0} - 1$, $1 - \bar{\mu}_{\text{apopt}}/\mu_{\text{apopt},0}$, and $\bar{\eta}/(\bar{\eta} + \eta_0)$. The means are computed for the population of cells within $r \leq 0.6$ to reduce the impact from boundary effects. We observe a selection pressure towards the activation of the hallmarks once the corresponding mutation is allowed, but also that the DNA damage and signaling imbalance mechanisms counteract hallmark progression. Hence the third hallmark constitutes a significant threshold for malignancy in the model.

Fig. 2 Mean hallmark status per cell at times corresponding to the vertical dashed lines in Fig. 1 at $t = 10, 120, 150, 210, 230$, and 260 , respectively, from left to right, top to bottom. Grey indicates empty voxels.

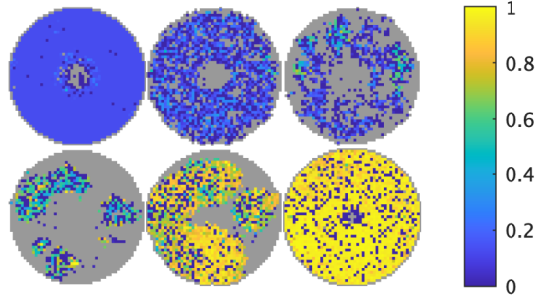


Fig. 2 visualizes the spatial concentration of hallmark phenotypes at selected times from the simulation. Thus, we can localize where hallmark progression occurs

to study the spatial components (if any) of both the reproductive potential and the selective pressure on the acquired phenotypes. For example, we observe that while some regions in the population initially progress faster towards hallmark achievements, progress ultimately spreads across the entire population. We also observe that population decline and growth correspond well with the proposed population reproduction number R_{pop} .

4 Discussion

Our aim with the paper was two-fold: to provide a foundation for understanding tumor evolution and to address ontological modeling uncertainties, thereby progressing towards a more comprehensive first-principles description of this intricate process.

To achieve our aim, we have interpreted the first four hallmarks of cancer as mechanisms in a general framework for cell population models. Through numerical experiments with locally exaggerated mutation rates and cellular turnover we observe the selective pressure within the studied time frame and a non-trivial progression towards hallmark capabilities, both in terms of population mean and phenotype spatial distributions. The results highlight the capacity of the model to test the impact of precisely defined hallmark capabilities on the cell population homeostasis, reproductive potential, and malignancy.

The results herein not only highlight the rich detail offered by computational spatial models of tumorigenesis, but is also suggestive of their potential to serve as pedagogic tools for approaching an intuitive understanding of the dynamics of tumors. Our work emphasizes the importance of balancing modeling granularity with a holistic view to shed light on the fundamental steps towards malignancy.

4.1 Availability and reproducibility

The computational results and figures can be reproduced with release 1.4 of the URDME open-source simulation framework [4], available for download at www.urdme.org (see the avascular tumor example and the associated README in the DLCM workflow).

Competing Interests This study was partially funded by the Swedish Research Council [grant number 2019-03471]. The authors have no conflicts of interest to declare that are relevant to the content of this chapter.

References

- [1] S. Benzekry, C. Lamont, A. Beheshti, A. Tracz, J. M. Eboš, L. Hlatky, and P. Hahnfeldt. Classical mathematical models for description and prediction of experimental tumor growth. *PLoS Comput. Biol.*, 10(8):e1003800, 2014. doi: 10.1371/journal.pcbi.1003800.
- [2] E. Blom and S. Engblom. Morphological stability for *in silico* models of avascular tumors, 2023. Available at <https://doi.org/10.48550/arXiv.2309.07889>.
- [3] G. W. Brodland. How computational models can help unlock biological systems. In *Semin. Cell Dev. Biol.*, volume 47, pages 62–73, 2015. doi: 10.1016/j.semcdb.2015.07.001.
- [4] B. Drawert, S. Engblom, and A. Hellander. URDM: a modular framework for stochastic simulation of reaction-transport processes in complex geometries. *BMC Syst. Biol.*, 6(76):1–17, 2012. doi: 10.1186/1752-0509-6-76.
- [5] R. Eftimie, J. L. Bramson, and D. J. Earn. Interactions between the immune system and cancer: a brief review of non-spatial mathematical models. *Bull. Math. Biol.*, 73:2–32, 2011. doi: 10.1007/s11538-010-9526-3.
- [6] S. Engblom, D. B. Wilson, and R. E. Baker. Scalable population-level modelling of biological cells incorporating mechanics and kinetics in continuous time. *R. Soc. Open Sci.*, 5(8):180379, 2018. doi: 10.1098/rsos.180379.
- [7] D. Hanahan. Hallmarks of cancer: New dimensions. *Cancer Discovery*, 12: 31–46, 1 2022. doi: 10.1158/2159-8290.CD-21-1059.
- [8] D. Hanahan and R. A. Weinberg. The hallmarks of cancer. *Cell*, 100(1):57–70, 2000. doi: 10.1016/S0092-8674(00)81683-9.
- [9] D. Hanahan and R. A. Weinberg. Hallmarks of cancer: the next generation. *Cell*, 144(5):646–674, 2011. doi: 10.1016/j.cell.2011.02.013.
- [10] C. Sonnenschein and A. M. Soto. The aging of the 2000 and 2011 hallmarks of cancer reviews: A critique. *Journal of Biosciences*, 38:651–663, 9 2013. doi: 10.1007/s12038-013-9335-6.
- [11] S. Whitaker. Flow in porous media i: A theoretical derivation of Darcy’s law. *Transp. Porous Media*, 1(1):3–25, 1986. doi: 10.1007/BF01036523.